Estonian Journal of Earth Sciences
2026, **75**, 2, 148–161

https://doi.org/10.3176/earth.2026.09

www.eap.ee/earthsciences
Estonian Academy Publishers

RESEARCH ARTICLE

Received 29 August 2025
Accepted 9 September 2026
Available online 15 October 2026

Keywords:
geochemistry, magnetite, trace elements, Jõhvi magnetic anomaly, banded iron formation, alteration

Corresponding author:
Siim Nirgi
siim.nirgi@yahoo.com

Citation:
Nirgi, S., Ratt, A., Maala, L., Paaver, P., Soesoo, A. and Kirsimäe, K. 2026. Trace elements in magnetite from the Jõhvi magnetite-rich gneisses in northeastern Estonia: implications for the genesis and alteration of iron mineralisation. *Estonian Journal of Earth Sciences*, **75**(2), 148–161. https://doi.org/10.3176/earth.2026.09

© 2026 Authors. This is an open access article distributed under the terms and conditions of the Creative Commons Attribution (CC BY) license (http://creativecommons.org/licenses/by/4.0).

Trace elements in magnetite from the Jõhvi magnetite-rich gneisses in northeastern Estonia: implications for the genesis and alteration of iron mineralisation

Siim Nirgi[a,b], Alvar Ratt[a], Lennart Maala[a,b], Peeter Paaver[a], Alvar Soesoo[a,b,c] and Kalle Kirsimäe[a]

[a] Department of Geology, University of Tartu, Ravila 14A, 50411 Tartu, Estonia
[b] Geological Survey of Estonia, F. R. Kreutzwaldi 5, 44314 Rakvere, Estonia
[c] Institute of Geology, Tallinn University of Technology, Ehitajate tee 5, 19086 Tallinn, Estonia

ABSTRACT

The study aimed to determine the origin of iron mineralisation in the crystalline basement beneath the Jõhvi magnetic anomaly through the trace element geochemistry of magnetite. Magnetite-bearing samples from mineralised intervals were examined petrographically, and the trace element compositions of magnetite grains were characterised using scanning electron microscopy and laser ablation inductively coupled plasma mass spectrometry. The results show that magnetite trace element compositions cluster into distinct groups depending on the host rock. The Jõhvi magnetite ore most likely formed as a banded iron formation deposit. However, its trace element signature has been significantly altered by later metamorphic and hydrothermal processes. These results highlight that magnetite trace element analysis alone cannot reliably determine the origin of iron ore deposits that have undergone strong alteration.

1. Introduction

Magnetite forms through a variety of geological processes, including chemical precipitation in sedimentary environments, magmatic crystallisation, hydrothermal alteration, metamorphism, and weathering. Among its occurrences, banded iron formations (BIFs) represent the most common and abundant magnetite deposits, consisting of alternating layers of chemically precipitated quartz and iron-rich sediments (Klein 2005; Hagemann et al. 2016; Konhauser et al. 2017). In iron oxide–copper–gold (IOCG) deposits, magnetite may occur either as a primary mineral or as a product of hydrothermal alteration (Skirrow 2022). Similarly, magnetite is found in porphyry Cu deposits, both as a primary phase and as a hydrothermal alteration product. Volcanogenic massive sulphide (VMS) deposits may also contain variable amounts of magnetite, typically associated with base metal sulphides such as Cu, Zn, and Pb (Yıldırım et al. 2016). Skarn deposits can host magnetite formed as a result of contact-metamorphism-induced metasomatic processes involving the interaction of hydrothermal fluids with carbonate rocks (Beaudoin et al. 2005). Magnetite also occurs in hydrothermal vein systems associated with diverse mineralisation styles, including Au, Ag, Cu, and base metals (Nadoll et al. 2014). In iron oxide–apatite (IOA) deposits, magnetite formation reflects a combination of igneous and magmatic-hydrothermal processes (Knipping et al. 2015). Additionally, magnetite is a common accessory mineral in metamorphic rocks, where it can form through the alteration of pre-existing minerals under high-temperature and high-pressure conditions (Jafari et al. 2019).

In the Estonian crystalline basement, several pronounced magnetic anomalies have been identified, most notably the Jõhvi magnetic anomaly (JMA), which reaches values of up to 19 300 nT (Plado et al. 2020). This anomaly was first detected in the early 1930s during military topographic mapping of magnetic declination (Linari 1940). Detailed geophysical investigations and an initial drilling campaign were conducted between 1935 and 1939, resulting in two deep drill holes (Jõhvi-I and Jõhvi-II) that

intersected magnetite-bearing gneisses within the crystalline basement at a depth of ca 200 m (Linari 1940). Subsequent exploration resumed in the 1960s, with additional gravimetric and magnetometric surveys conducted in 1961 and 1964–1965, followed by drilling in 1967–1968 (Erisalu et al. 1969; Suuroja 1969). More recently, exploration of the JMA resumed in 2019 (Nirgi et al. 2022).

These studies have revealed that the JMA is caused by subvertical magnetite-rich layers within garnet–cordierite and pyroxene gneisses of the crystalline basement, located beneath approximately 240 m of sedimentary cover and potentially extending to depths of up to 1000 m (Linari 1940; Erisalu et al. 1969; Plado et al. 2020; Soesoo et al. 2021; Nirgi et al. 2022). However, the magnetite-bearing rocks of the JMA display a wide range of textural features and major-element compositions, making their classification as a specific deposit type uncertain (Soesoo et al. 2021).

According to Dupuis and Beaudoin (2011), trace elements that substitute for Fe in the magnetite crystal lattice can be grouped based on their chemical properties and structural behaviour. These substitutions have been successfully used to distinguish magnetite associated with a wide range of deposit types, including IOCG, Kiruna-type apatite–magnetite, BIF, porphyry Cu, Fe–Cu skarn, Fe–Ti, V, Cr, Ni–Cu–PGE, Cu–Zn–Pb VMS, Archaean Au–Cu porphyry, and Opemiska-type Cu vein deposits (Dupuis and Beaudoin 2011; Dare et al. 2014; Nadoll et al. 2014; Knipping et al. 2015). Consequently, the trace element composition of magnetite serves as a geochemical fingerprint of its physicochemical formation environment and enables the discrimination of genetic ore types (Dupuis and Beaudoin 2011). The trace element composition of magnetite from the JMA was preliminarily investigated in selected legacy core samples by Soesoo et al. (2021), but that study did not yield a conclusive interpretation regarding the origin of the magnetite. In this study, we present a systematic in situ trace element analysis of magnetite from iron-ore-bearing intervals in the JMA with the aim of constraining the genetic classification of the magnetite mineralisation in this region.

2. Geological setting

The Palaeoproterozoic to Mesoproterozoic crystalline basement of Estonia is predominantly composed of Svecofennian metamorphic and plutonic formations, along with anorogenic rapakivi granites that intrude the older Svecofennian metamorphic complex (Puura et al. 1996). This basement, structurally equivalent to the Svecofennian Domain of the Fennoscandian Shield, is characterised by a gently southward-dipping peneplain surface, inclining at a rate of approximately 2–4 m/km. It is entirely covered by a sedimentary sequence ranging in thickness from approximately 100 m in northern Estonia to around 800 m in the south and southwest (Fig. 1). Consequently, no outcrops of crystalline basement are exposed on the Estonian mainland.

Structurally, the Estonian crystalline basement is divided into a northern amphibolite-facies domain and a southern granulite-facies domain, separated by the Paldiski–Pskov deformation zone (Puura et al. 1996; Soesoo et al. 2004; Solano-Acosta et al. 2023). Based on petrological and geophysical characteristics, six structural zones are recognised: Tallinn, Alutaguse, Jõhvi, Tapa, West Estonian, and South Estonian.

The Jõhvi Zone, which hosts the JMA, is a narrow belt approximately 20–30 km wide and 100 km long in northeastern Estonia. The basement rocks of the Jõhvi Zone comprise migmatised gneisses and granites of varying compositions, including pyroxene gneisses, quartz–feldspar gneisses, biotite–plagioclase gneisses, amphibole gneisses, garnet–cordierite gneisses, and magnetite-rich gneisses and quartzites, collectively referred to as the Vaivara Complex (Koppelmaa et al. 2002; Soesoo et al. 2004).

According to Soesoo et al. (2021), these rocks have experienced metamorphism under granulite-facies conditions, and the bedding of both magnetite-rich and barren gneisses is predominantly subvertical. Metamorphic temperatures, as estimated using the garnet–biotite geothermometer, range between 650 °C and 750 °C, while pressure estimates derived from the garnet–biotite–plagioclase–quartz geobarometer range from 2.9 to 4.9 kbar (Soesoo et al. 2021).

The JMA is characterised by several local magnetic maxima, the strongest reaching 19 300 nT in the western anomaly, and is accompanied by weak positive gravity anomalies (Plado et al. 2020). The JMA magnetite-rich gneisses and quartzites occur within the western anomaly as predominantly subvertical beds hosted by garnet–cordierite and pyroxene gneisses and intercalated with numerous migmatitic granites. The mineralised zones consist predominantly of magnetite and magnetite–sulphide assemblages. Individual magnetite-bearing intervals intersected in drill holes have apparent downhole thicknesses of up to 34.6 m. Because the mineralised units are predominantly subvertical, all reported thicknesses represent apparent drill-core intersection lengths rather than true structural thicknesses. The cumulative apparent thickness of magnetite and magnetite–sulphide mineralised intervals reaches approximately 208 m in borehole PA1 and 257 m in borehole PA2, whereas the cumulative true thickness of the western anomaly orebody has been estimated at approximately 100 m (Nirgi et al. 2022).

Previous studies have correlated the Jõhvi Zone and the surrounding North Estonian basement with the broader Bergslagen–Uusimaa–North Estonia tectonic belt, based on petrological, geochemical, and geochronological similarities across the Baltic Sea region (Bogdanova et al. 2015; Sundblad et al. 2021). The Jõhvi Zone has also been interpreted as geologically comparable to the Bergslagen region of central Sweden and possibly to the Orijärvi area in southern Finland (Nirgi and Soesoo 2021).

3. Materials and methods

In this study, 17 bulk-rock samples were selected from the PA1 and PA2 drill cores drilled in 2019 (Fig. 2; Table 1). The selected samples represent magnetite-bearing intervals from different mineralised zones and were chosen to represent the variety of host-rock mineral assemblages present within the

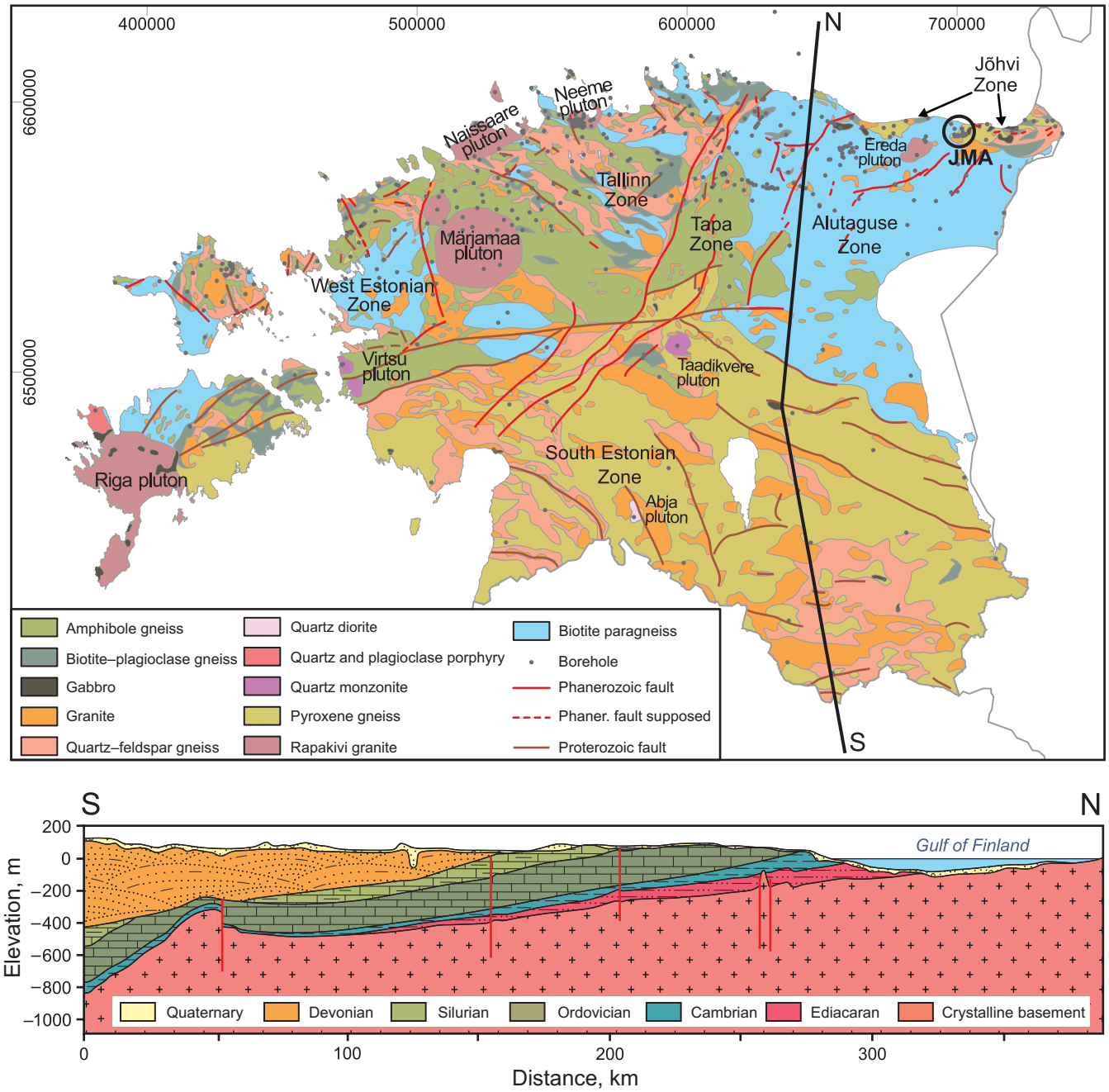

Fig. 1. Geological map of the Estonian crystalline basement (Koppelmaa et al. 2002) and a cross-section illustrating the sedimentary cover, the buried crystalline basement, and the southward-dipping basement surface (modified after Vaher et al. 1962).

JMA (Fig. 3). The mineralogical composition of the host rocks was determined using a combination of previously published and newly acquired petrographic data. The geochemical composition and mineralogical descriptions of the host-rock types, based on thin-section petrography and X-ray diffraction analyses, were previously reported by Nirgi et al. (2022). Host-rock groups were assigned according to the dominant mineral assemblages identified in each sample, with minerals listed in decreasing order of abundance in Table 1.

Thin sections and polished slabs were inspected and photographed using binocular and optical polarising microscopes in transmitted and reflected light, and using a scanning electron microscope (SEM) with backscattered electron (BSE) imaging. The SEM was a ZEISS EVO MA15 equipped with an Oxford AZTEC-MAX energy-dispersive (EDS) system. Trace element concentrations were measured by laser ablation inductively coupled plasma mass spectrometry (LA-ICP-MS) using an Agilent 8800 quadrupole ICP-MS coupled to a Cetac LSX-213 G2+ Nd:YAG laser with a HelEx II fast-washout two-volume large-format cell and a 'squid' smoothing interface at the University of Tartu.

Spot analyses on the samples were performed using the following laser parameters: a fluence of 3.2 J/cm^2, a repetition rate of 10 Hz, and a 50 µm round spot. He was used as a carrier gas at a flow rate of 800 mL/min. A 20 s gas blank was collected before each ablation pass, and the ablation signal was collected for 45 s. USGS GSD1G and BCR2G were used as the calibration and secondary quality control standards, respectively, and were measured in triplicate after every 20 sample ablations. The oxide formation ratio, expressed as ThO/Th during the ablation of NIST 610 during instrument tuning, was < 0.25%. Signals of ^{24}Mg, ^{27}Al, ^{28}Si,

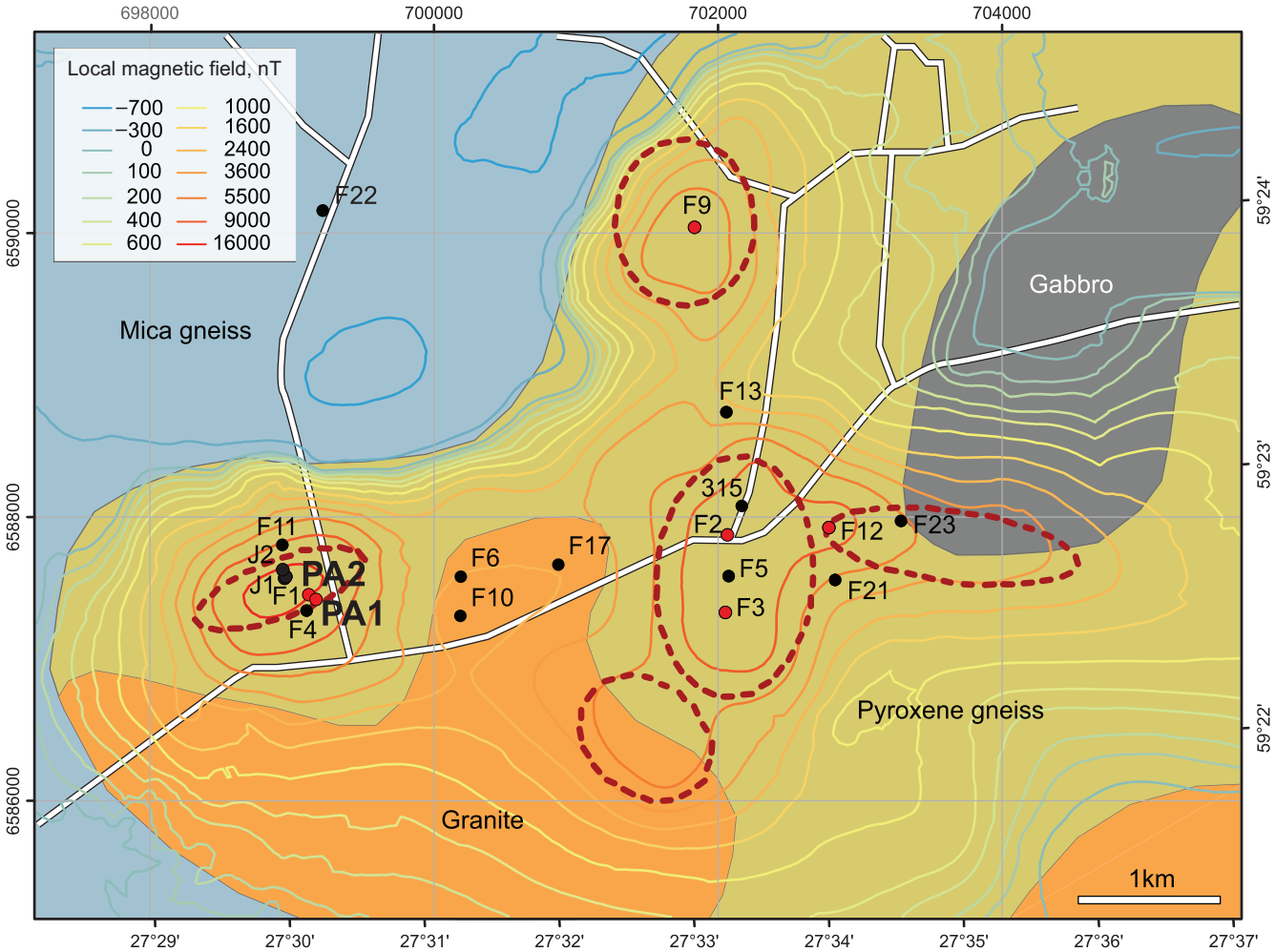

Fig. 2. Geological map of the crystalline basement of the Jõhvi magnetic anomaly and the locations of all deep drill holes, including PA1 and PA2 studied here (Linari 1940; Erisalu et al. 1969; Koppelmaa et al. 2002; Nirgi et al. 2022). The red dots show drill holes where magnetite-rich gneiss has been intersected. Total local magnetic intensity is presented as contours, and the surface projection of the modelled potential orebodies as red dashed lines (modified after Plado et al. 2020). Coordinates are in L-EST97 (EPSG:3301) and WGS 84 (EPSG:4326).

Table 1. Host-rock types of the analysed magnetite samples and their designated groups used in data analysis. Mineral abbreviations: Qz – quartz, Kfs – K-feldspar, Bt – biotite, Pl – plagioclase, Fsp – feldspar, Grt – garnet, Px – pyroxene, Amp – amphibole, Mag – magnetite, Py – pyrite, Po – pyrrhotite. Minerals are listed in decreasing order of abundance

Sample	Borehole	Depth, m	Mineralogy	Group
P1-01	PA1	317.4	Qz–Kfs–Bt–Pl	Fsp-rich
P1-02	PA1	343.7	Qz–Kfs–Bt–Pl	Fsp-rich
P1-03	PA1	456.9	Pl–Qz–Kfs–Bt	Pl-rich
P1-04	PA1	511.0	Px–Qz–Grt	Grt–Px-rich
P1-05	PA1	562.0	Qz–Pl–Amp–Bt–Grt	Grt-rich
P1-06	PA1	726.5	Qz–Pl–Bt–Px	Fsp-rich
P2-01	PA2	447.3	Qz–Grt–Py–Po	Grt-rich
P2-02	PA2	455.3	Px–Qz–Grt	Grt–Px-rich
P2-03	PA2	474.7	Qz–Pl–Px–Amp–Grt	Grt–Px–Pl-rich
P2-04	PA2	497.8	Px–Po–Qz–Grt	Grt–Px-rich
P2-05	PA2	562.05	Qz–Mag–Grt–Bt	Grt-rich
P2-06	PA2	562.14	Qz–Mag–Grt–Bt	Grt-rich
P2-07	PA2	593.3	Qz–Px–Mag–Grt	Grt–Px-rich
P2-08	PA2	629.0	Qz–Mag–Amp–Bt–Px	Px–Amp-rich
P2-09	PA2	629.8	Qz–Mag–Amp–Bt–Px	Px–Amp-rich
P2-10	PA2	678.7	Mag–Amp–Px–Qz	Px–Amp-rich
P2-11	PA2	736.8	Qz–Grt–Fsp–Mag	Fsp-rich

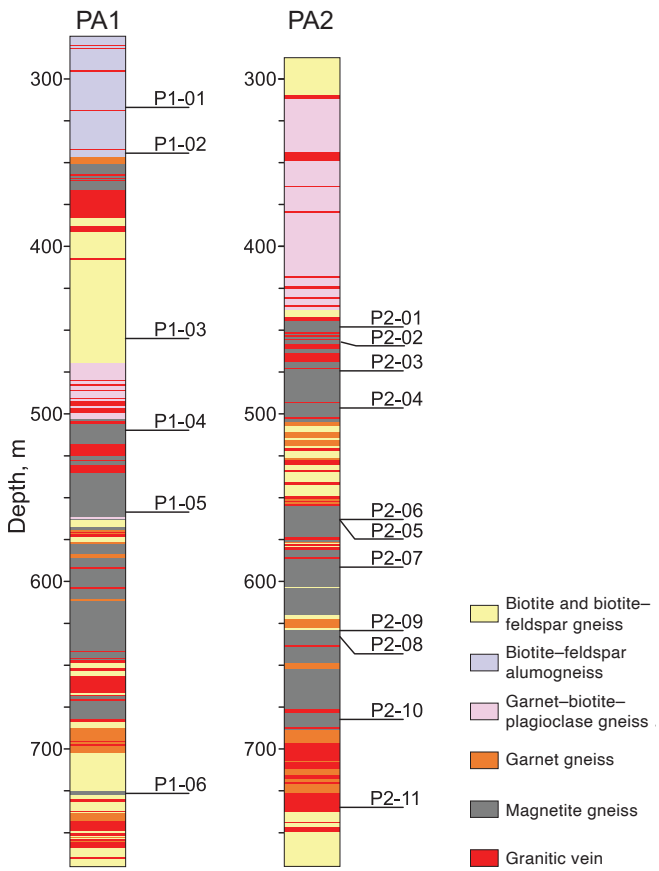

Fig. 3. Schematic drill-core profiles of PA1 and PA2 showing lithological units and locations of the studied samples (P1-01–P1-06 and P2-01–P2-11). Thicknesses correspond to apparent drill-core intersection lengths of predominantly subvertical lithological units.

^{29}Si, ^{43}Ca, ^{47}Ti, ^{49}Ti, ^{51}V, ^{52}Cr, ^{55}Mn, ^{59}Co, ^{60}Ni, ^{66}Zn, ^{71}Ga, ^{72}Ge, ^{73}Ge, ^{90}Zr, ^{95}Mo, and ^{118}Sn were collected with a dwell time of 6 ms, the ^{63}Cu signal was collected with a dwell time of 10 ms, and the ^{208}Pb signal was collected with a dwell time of 20 ms, amounting to a total duty cycle of 0.3 s on the ICP-MS. Trace element concentrations measured in quality control samples were within 5% of the reference values throughout the analytical sessions.

Data reduction of the raw signals was performed using iolite v4. After background subtraction, concentrations were calculated using the X-Trace Elements internal standard data reduction scheme, with quantitative standardisation based on Fe as the internal standard element.

Fe concentrations in magnetite grains were measured using a ZEISS EVO MA15 SEM equipped with an Oxford AZTEC-MAX EDS system at an acceleration voltage of 15 kV, a probe current of 10 nA, a defocused beam, and an acquisition time of 40 s. Natural magnetite and haematite from the EM-Tec RXS-40MC mineral reference standard were used for calibration and quality control, respectively. The relative precision of iron oxide measurements was 0.2%. Fe concentrations in magnetite grains were used as internal standard values for LA-ICP-MS data reduction. Because of numerous silicate and other mineral impurities/inclusions, the LA-ICP-MS raw data were filtered, and data with a K content of over 500 mg/kg or with both Ca and Al contents of over 10 000 mg/kg were excluded from further analysis. Median values were calculated for measurement points within the same grain. Altogether, data from 115 magnetite grains were analysed. Principal component analysis (PCA) of magnetite trace element data was performed using the CoDaPack code, which applies a log-ratio transformation to the data prior to PCA to open the otherwise closed compositional datasets (Aitchison et al. 2000).

4. Results

4.1. Magnetite petrography

The elevated magnetite content within the JMA is predominantly observed in several gneissic rock types (Fig. 4A–H), including garnet–pyroxene gneiss, pyroxene–garnet gneiss, pyroxene gneiss, garnet–amphibole gneiss, garnet–biotite–feldspar gneiss, and amphibole–garnet gneiss. In these rocks, magnetite-rich foliated beds or layers alternate with quartz-rich bands or layers dominated by mafic minerals, forming a distinct banded structure (Fig. 4I).

In drill cores PA1 and PA2, mineralisation is primarily characterised by xenoblastic magnetite grains. These occur either as elongated grains (1–3 mm) aligned with the foliation (Fig. 5A) or as discrete, rounded xenoblastic grains ranging from 20 to 100 µm, set within a silicate matrix (Fig. 5B).

In andalusite- and/or sillimanite–cordierite-bearing biotite–feldspar gneisses, magnetite occurs as mesoblastic, elongated grains up to 1.5 mm long, aligned parallel to the rock foliation, particularly within sillimanite-rich layers. A similar texture is observed in magnetite–garnet–biotite–amphibole–plagioclase gneisses, where magnetite coexists with sulphides, as well as in chlorite-bearing garnet–magnetite gneisses and garnet–magnetite–pyroxene gneisses (Fig. 5C). In these rocks, magnetite commonly forms irregular xenoblastic grains aligned with foliation, embedded within a silicate matrix. In pyroxene–amphibole–magnetite gneisses, magnetite is frequently concentrated in distinct bands composed of elongated crystals, commonly containing garnet and pyroxene inclusions (Fig. 5D).

4.2. Trace element composition of magnetite

The trace element composition of magnetite from the JMA is presented in Fig. 6 and Table S1 (see Supplementary online data). Based on the mineralogical composition of the host rocks, the magnetite samples were assigned to six host-rock categories: Fsp-rich, Grt-rich, Grt–Px-rich, Grt–Px–Pl-rich, Pl-rich, and Px–Amp-rich host-rock types (see Table 1 for mineral abbreviations).

The most abundant trace elements in magnetite from the JMA are V, Cr, Ni, Ti, and Mn, although their concentrations show substantial variability. V concentrations range from 20 to 3672 mg/kg. The highest concentrations occur in magnetite from Fsp-rich host rocks, with V values ranging from 398 to 3672 mg/kg and a median of 534 mg/kg. In other host-rock types, V concentrations range from 20 to 260 mg/kg. Mn exhibits the greatest variability among the trace elements, ranging from 178 to 19 259 mg/kg. The most Mn-enriched magnetite is found in Grt–Px-rich host rocks, where Mn concentrations range from 1680 to 19 259 mg/kg, with a notably

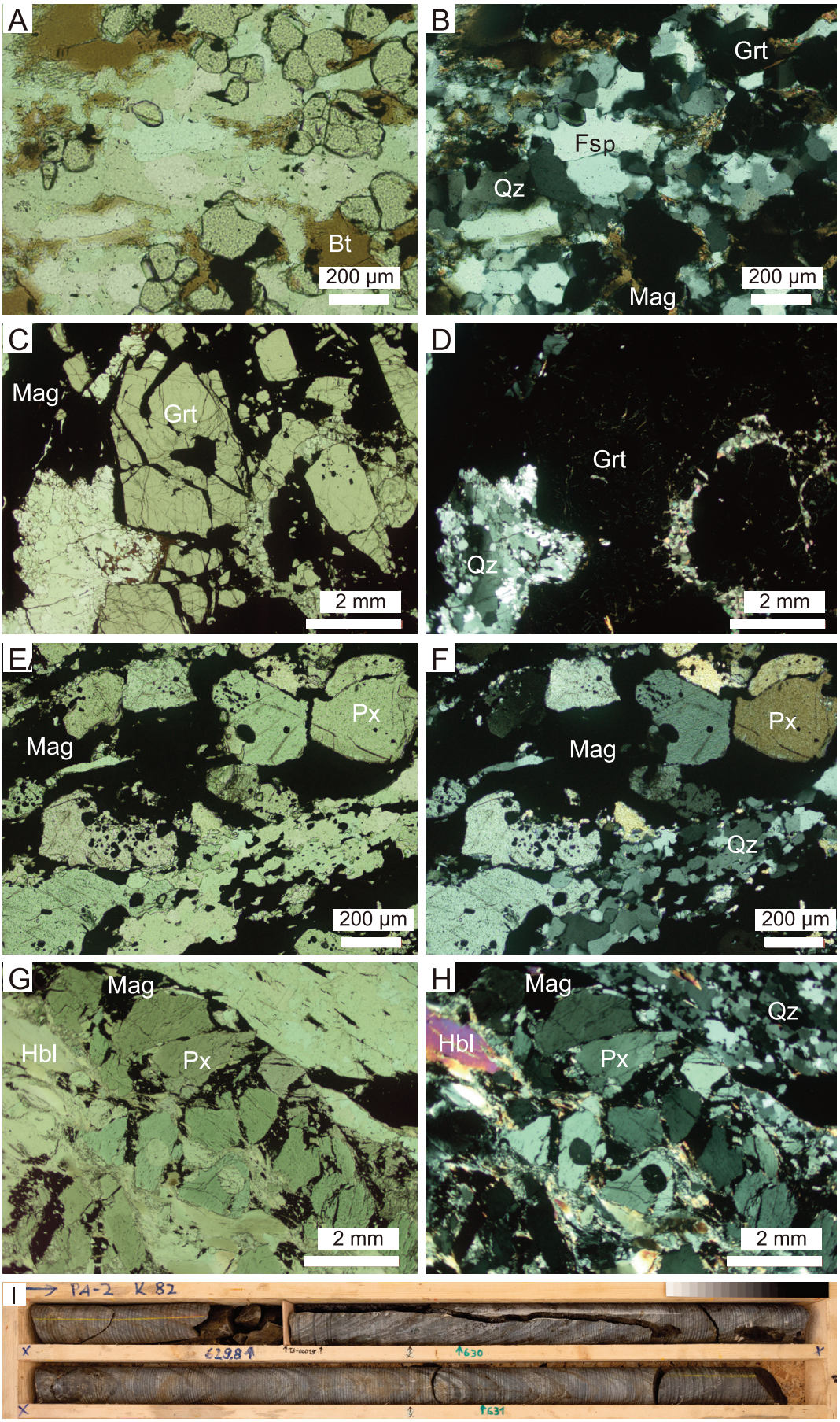

Fig. 4. Photomicrographs (A–H) of the main magnetite host-rock types. Feldspar-rich rock: (A) in plane-polarised light (PPL) and (B) under crossed polars (XPL), core PA2, 736.8 m; garnet-rich rock: (C) in PPL and (D) under XPL, core PA1, 456.9 m; garnet–pyroxene-rich rock: (E) in PPL and (F) under XPL, core PA2, 592.8 m; pyroxene–amphibole-rich rock: (G) in PPL and (H) under XPL, core PA2, 629.8 m. Photograph (I) of magnetite-bearing amphibole–pyroxene gneiss with characteristic foliated magnetite banding in drill core PA2, at a depth of 630 m. Abbreviations: Bt – biotite, Fsp – feldspar, Grt – garnet, Hbl – hornblende, Mag – magnetite, Px – pyroxene, Qz – quartz. Photos by Siim Nirgi.

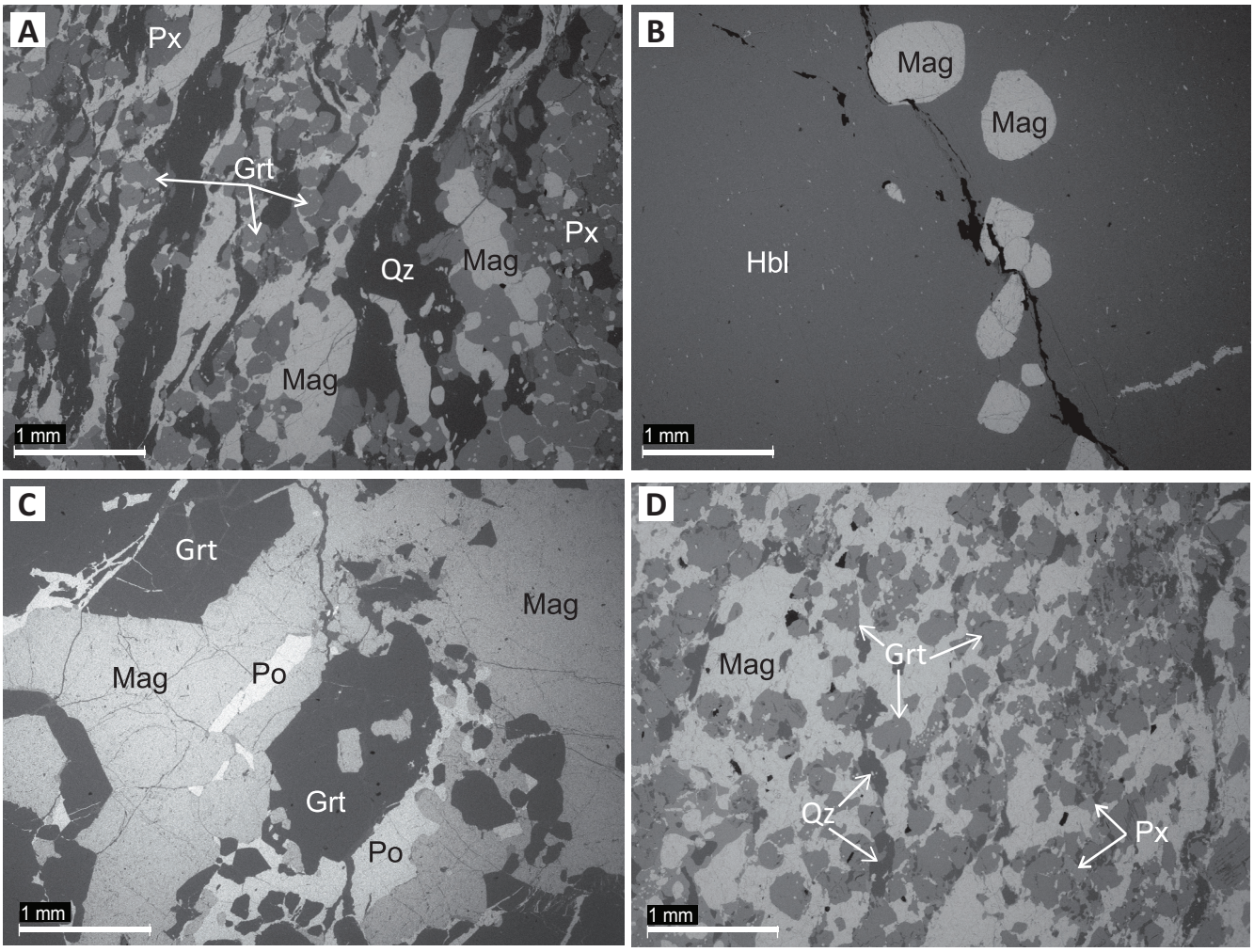

Fig. 5. Backscattered electron images of Mag grains in JMA rocks: (A) xenoblastic Mag grains in Grt–Mag gneiss, sample P2-06, core PA2, at a depth of 562.14 m; (B) rounded Mag grains in Bt-bearing Amp–Mag gneiss, sample P2-09, core PA2, at a depth of 629.82 m; (C) Mag with a Po inclusion in chloritised Grt–Mag gneiss, sample P2-01, core PA2, at a depth of 447.32 m; (D) Mag band (~10 mm wide) in Grt–Mag–Px gneiss, sample P2-02, core PA2, at a depth of 455.32 m. Abbreviations: Amp – amphibole, Bt – biotite, Grt – garnet, Hbl – hornblende, Mag – magnetite, Po – pyrrhotite, Px – pyroxene, Qz – quartz.

high median of 12 925 mg/kg. In other host rocks, Mn concentrations range from 178 to 8469 mg/kg. Co concentrations range from 1 to 141 mg/kg. Similar to Mn, Co is enriched in Grt–Px-rich host rocks, with concentrations between 1 and 141 mg/kg (median: 63 mg/kg), while magnetite from other lithologies generally contains less than 78 mg/kg. Ga concentrations range from 1 to 330 mg/kg, with the highest concentrations (145–196 mg/kg) in Pl-rich samples. Both Co and Ga exhibit systematically lower concentrations in magnetite associated with sulphide phases, especially in Grt–Px-rich and Px–Amp-rich host rocks (Table S1).

Cr concentrations vary considerably, from 1 to 7248 mg/kg, with the highest Cr enrichment in Fsp-rich host rocks (median: 915 mg/kg). Al concentrations range from 245 to 13 300 mg/kg (median: 2625 mg/kg), and Mg concentrations range from 11 to 1513 mg/kg (median: 527 mg/kg). Ni concentrations range from 0.4 to 218 mg/kg, with the highest values observed in Fsp-rich host rocks (87–218 mg/kg; median: 141 mg/kg). In other host-rock types, Ni concentrations do not exceed 48 mg/kg. Ti concentrations range from 116 to 10 309 mg/kg. Pl-rich rocks contain the most Ti-enriched magnetite, with values ranging from 1759 to 9257 mg/kg (median: 3299 mg/kg). Cu concentrations are low, ranging from 0.02 to 5 mg/kg. The highest Cu concentrations are found in Grt-rich host rocks, with values ranging from 0.3 to 5 mg/kg and a median of 4 mg/kg. Zn exhibits considerable variability, ranging from 4 to 1835 mg/kg across all sample types. Mo, Ag, and Sn are generally present in low concentrations (< 50 mg/kg); however, Sn reaches concentrations of up to 175 mg/kg in Pl-rich host rocks.

5. Discussion

The origin of the JMA has been debated extensively, with several earlier hypotheses proposed: Linari (1940) suggested a skarn-like origin, Vaganova and Kadyrova (1948) proposed a metasomatic genesis, and Tikhomirov (1966) described complex metamorphic assemblages cut by granite veins. Later studies argued that the JMA formed during regional metamorphism of a volcanogenic–sedimentary sequence, involving recrystallisation and alteration of pre-existing iron-bearing minerals (Puura and Kuuspalu 1966; Erisalu et al. 1969). More recently, Soesoo et al. (2020) noted geological similarities between the JMA and deposits in the Bergslagen region

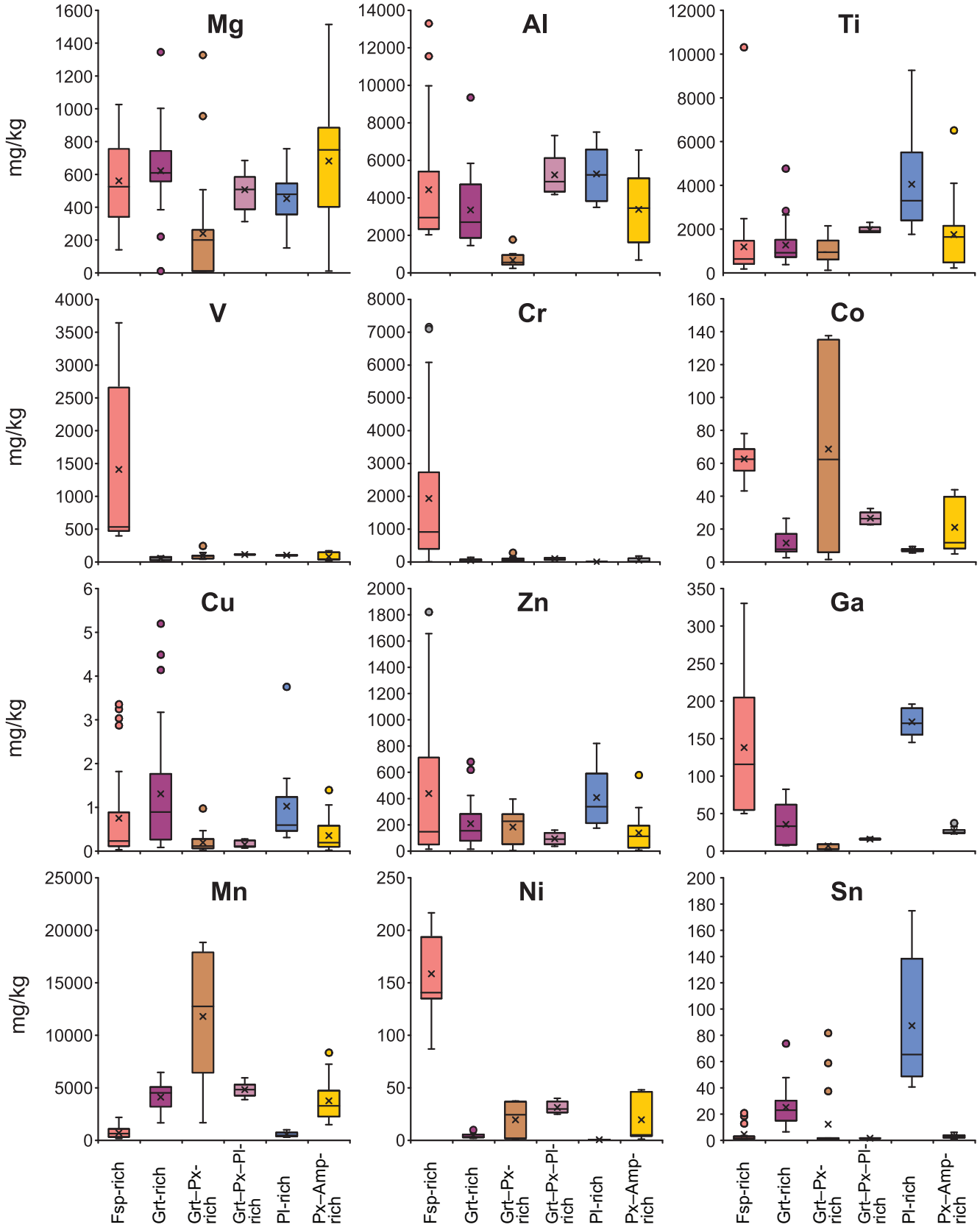

Fig. 6. Variations in selected trace element concentrations in magnetite from different JMA host-rock groups: Fsp-rich, Grt-rich, Grt–Px-rich, Grt–Px–Pl-rich, Pl-rich, and Px–Amp-rich. Complete analytical data are provided in Table S1 in the Supplementary online data.

of Sweden. However, despite all these earlier studies, the origin of the JMA has remained unresolved.

Because the JMA mineralisation has undergone high-grade metamorphism and migmatisation, it is first necessary to evaluate whether the trace element composition of magnetite mainly reflects the original ore-forming process or later modification. Therefore, the influence of host-rock composition on magnetite chemistry is examined before applying deposit discrimination schemes and genetic classification models.

5.1. Host-rock control and secondary overprinting

The trace element composition of Jõhvi magnetite varies systematically with host-rock type. Figure 6 and the PCA results (Fig. 7) demonstrate that magnetite from Fsp-rich, Pl-rich, and Grt–Px-rich rocks forms distinct compositional populations. This separation indicates that host-rock mineralogy exerts a systematic control on magnetite trace element composition. Fsp-rich-hosted magnetite plots mainly towards the negative principal component (PC1) direction and is associated with elevated Ni, Cr, and V concentrations, with some analyses also trending towards the Co vector. Pl-rich-hosted magnetite forms a distinct population towards positive PC1 and is associated with elevated Sn and Mo concentrations. Magnetite from Grt-rich, Grt–Px-rich, and related host rocks is mainly separated along PC2 and is characterised by elevated Mn concentrations. These group-specific compositional differences correspond closely to the present host-rock assemblages and indicate that magnetite chemistry must be interpreted in the context of host-rock evolution rather than solely as a primary ore-forming signal.

Nevertheless, some trace element variability may have been inherited from primary or syngenetic hydrothermal processes during the formation of the iron-rich precursor. This possibility is particularly relevant if the original mineralisation formed in a volcanogenic hydrothermal environment. The elevated Sn and Mo concentrations observed in Pl-rich-hosted magnetite may reflect hydrothermal fluid–rock interaction and redistribution of mobile trace elements during post-depositional alteration (Heinrich 2007). However, the systematic correspondence between magnetite chemistry and the present host-rock assemblages, together with the Fsp-rich and Grt–Px-rich mineralogical associations, indicates that later metamorphic and metasomatic processes exerted a major control on the preserved magnetite compositions.

5.2. Relative alteration of the host-rock groups

The different magnetite populations identified in this study also appear to reflect varying degrees of secondary modification. Magnetite hosted by Fsp-rich rocks is interpreted as the most altered population. These rocks are strongly migmatised biotite–feldspar and biotite–quartz–feldspar gneisses, where K-feldspar and plagioclase form large porphyroblasts that constitute up to approximately 43% and 16% of the rock volume, respectively (Nirgi et al. 2022). In many cases, plagioclase is replaced by microcline, indicating extensive potassium metasomatism associated with high-temperature fluid

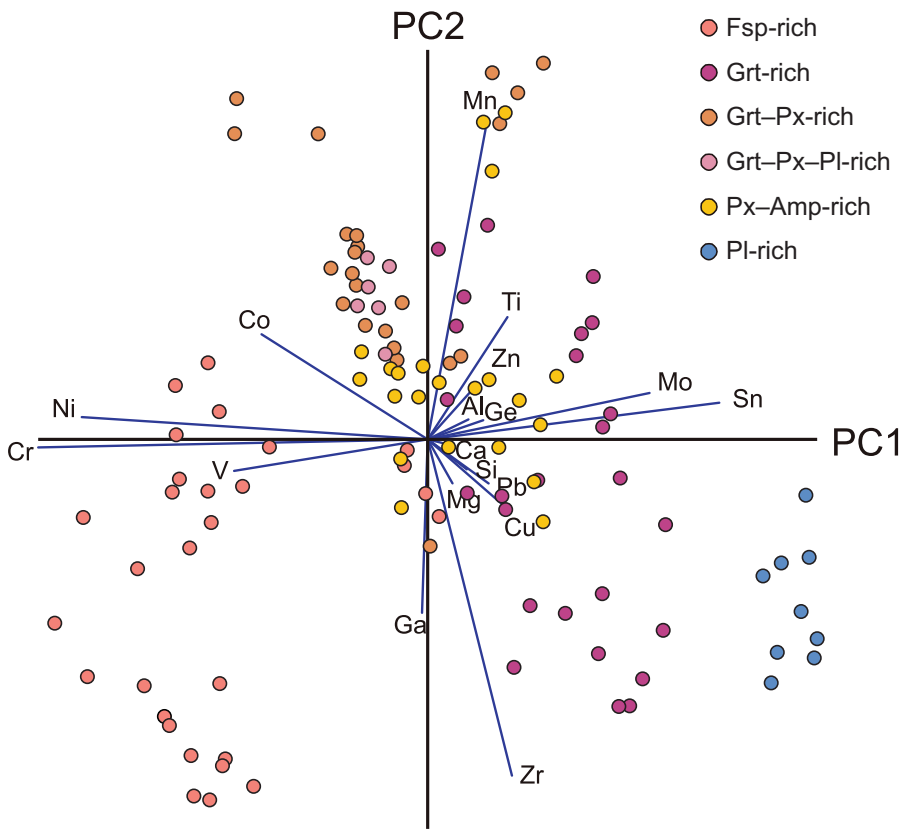

Fig. 7. Principal component analysis plot of the first and second principal components (PC1 and PC2) of centred log-ratio (clr)-transformed trace element concentrations in magnetite from the JMA. The plot illustrates the compositional separation of magnetite from the Fsp-rich, Pl-rich, and Grt–Px-rich host-rock groups. PC1 and PC2 together explain 55.1% of the total variance.

activity during syn- or post-orogenic migmatisation. Partial melting and associated fluid flux resulted in substantial reworking of the host rocks and likely modified the trace element composition of the associated magnetite.

In contrast, magnetite hosted by Grt–Px-rich rocks exhibits fewer indications of hydrothermal modification and is therefore interpreted as the least altered magnetite population within the JMA. Consequently, this group is considered the most likely to preserve trace element characteristics inherited from the original iron mineralisation.

5.3. Deposit discrimination diagrams in an overprinted system

The trace element geochemistry of magnetite provides a potential tool for investigating the genesis of Fe deposits. Dupuis and Beaudoin (2011) showed that trace elements that can replace Fe in the magnetite crystal structure can be categorised into different groups based on their chemical properties and behaviour within the crystal structure of magnetite. Common elements that can substitute for Fe in magnetite include transition metals such as Mn, Zn, Co, Cr, Ni, and Ti, which can replace Fe through solid-solution substitution and form various solid-solution series with magnetite. Elements such as Mg and Al can also substitute for Fe, forming magnesioferrite and aluminomagnetite solid solutions with magnetite, respectively. Other trace elements, including V and Ga, may likewise enter the magnetite lattice and influence its overall composition. All these substitutions allow discrimination of iron oxides between different mineral deposit types (Dupuis and Beaudoin 2011).

Because the trace element data show strong host-rock control, deposit discrimination diagrams are used here as comparative tools rather than as standalone genetic classifiers. On the Ti + V vs. Ni/(Cr + Mn) diagram (Fig. 8A; Dupuis and Beaudoin 2011), most JMA samples plot outside the established genetic fields, typically exhibiting lower Ni/(Cr + Mn) ratios than magnetite from typical skarn deposits. Only a few samples, primarily those from Fsp-rich host rocks, plot near the boundaries of the IOCG, porphyry, or Fe–Ti, V fields. A similar pattern is observed on the Ti + V vs. Ca + Al + Mn diagram (Fig. 8B), where Jõhvi magnetite generally falls outside the defined fields and displays lower Ti + V values than skarn-related magnetite. Magnetite from Fsp-rich, especially Pl-rich, host rocks is an exception, tending to plot within the porphyry field, with a subset also falling within the IOCG field. Notably, all previous magnetite trace element data reported by Soesoo et al. (2021) plot in the uppermost portion of the porphyry field.

Overall, these discrimination plots indicate that the trace element signature of magnetite from the JMA does not correspond to any single, well-defined deposit type. This finding implies either an unusual primary origin for the magnetite or overprinting of its original composition by later processes. In fact, Dupuis and Beaudoin (2011) observed that hydrothermal iron-oxide ores from many deposits worldwide display scattered trace element patterns across such diagrams, supporting the possibility that the chemistry of the magnetite was modified by hydrothermal alteration.

The partial overlap of magnetite compositions from the JMA with the skarn field in Fig. 8 is primarily controlled by elevated Mn concentrations, particularly in magnetite hosted by Mn-rich garnet–pyroxene rocks. These rocks are characterised by Mn-rich mineral assemblages, including spessartine-bearing garnets, and the associated magnetite commonly exhibits elevated Mn concentrations. Because Mn is a major component of the discrimination parameters used in Fig. 8, Mn-rich magnetite from the JMA plots towards the skarn field. However, the elevated Mn concentrations are regarded as a characteristic feature of the Jõhvi mineralised sequence and its host rocks rather than as evidence for a skarn-related mineralising event.

As noted by Nadoll et al. (2014), individual trace element enrichments may result from multiple geological processes; therefore, interpretation should rely on overall compositional patterns rather than single-element signatures. Following the discrimination scheme of Nadoll et al. (2014), the analysed magnetite samples and their host rocks can be divided into three broader compositional groups (Fig. 9):

(a) Fsp-rich host rocks: magnetite is characterised by elevated Al, Ti, V, Cr, Ni, and Co concentrations and displays the

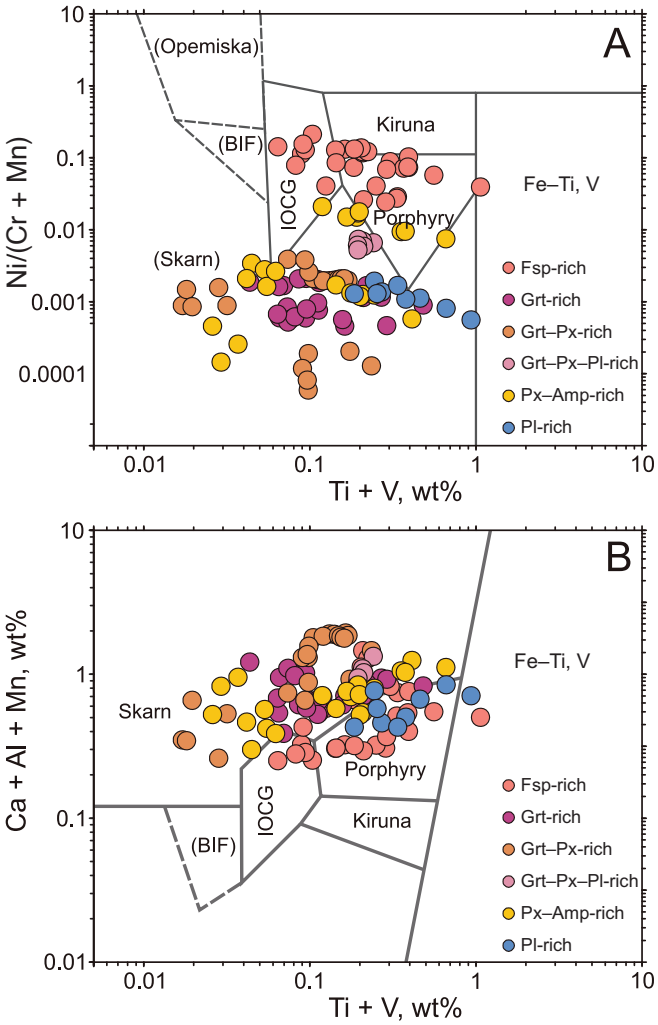

Fig. 8. Magnetite chemical composition on discrimination diagrams: (A) Ti + V vs. Ni/(Cr + Mn); (B) Ti + V vs. Ca + Al + Mn (after Dupuis and Beaudoin 2011). Abbreviations: BIF – banded iron formation, IOCG – iron oxide–copper–gold.

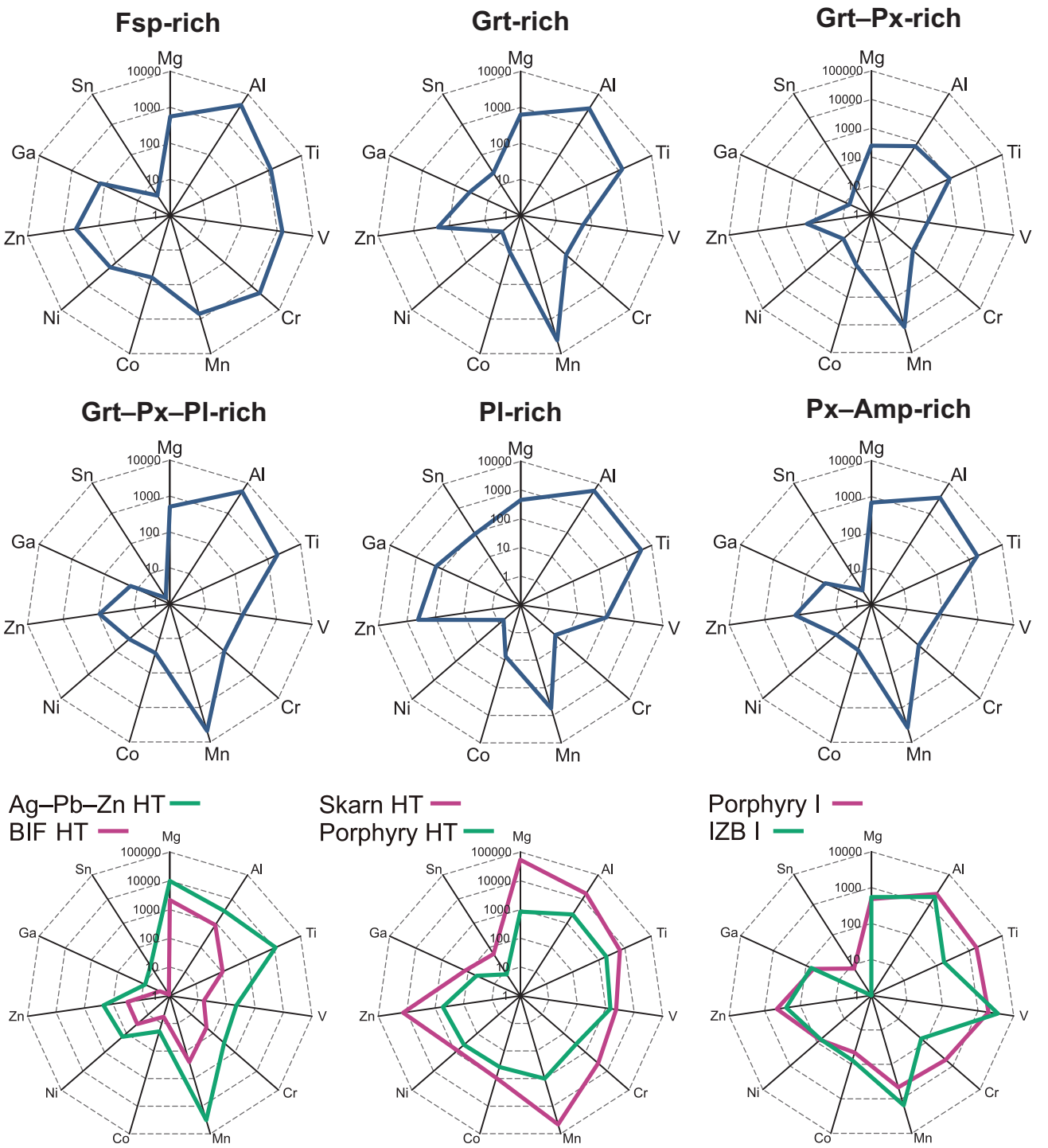

Fig. 9. Chemical composition of Jõhvi magnetite on discrimination radar diagrams after Nadoll et al. (2014). Abbreviations: Ag–Pb–Zn HT – hydrothermal Ag–Pb–Zn vein magnetite, BIF HT – hydrothermally modified BIF-related iron ore magnetite, IZB I – igneous magnetite from the unmineralised inner zone batholith, porphyry HT – hydrothermal porphyry-system magnetite, porphyry I – igneous porphyry-related magnetite, skarn HT – hydrothermal skarn magnetite.

closest affinity to hydrothermal and igneous magnetite from porphyry and skarn systems.

(b) Grt–Px-rich rocks: this group (including Grt-rich, Grt–Px-rich, Grt–Px–Pl-rich, and Px–Amp-rich host-rock types) is characterised by a pronounced Mn enrichment together with elevated Mg and generally low Ni and Co concentrations. Magnetite compositions show the closest affinity to hydrothermal BIFs.

(c) Pl-rich rocks: magnetite is characterised by elevated Ti, Zn, Ga, and Sn concentrations and shows the closest affinity to hydrothermal Ag–Pb–Zn vein deposits.

This interpretation is further supported by the criteria of Nadoll et al. (2015), who used Ti and V concentrations to distinguish igneous from hydrothermal magnetite in porphyry systems. Igneous magnetite is typically enriched in both Ti and V, although some overlap exists between the igneous and hydrothermal fields (Fig. 10). Magnetite hosted by Grt–Px-rich (± Pl or Amp) and Pl-rich rocks contains higher Ti concentrations than typical hydrothermal magnetite, yet its V concentrations (19–3672 mg/kg; median: ≈ 95 mg/kg) remain within the hydrothermal range. Magnetite in Fsp-rich rocks shows even higher V concentrations, overlapping with the

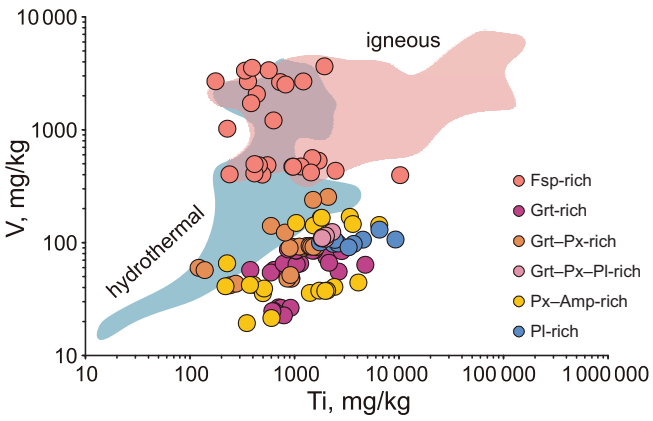

Fig. 10. Ti and V concentrations in Jõhvi magnetite, with fields for hydrothermal and igneous magnetite after Nadoll et al. (2015).

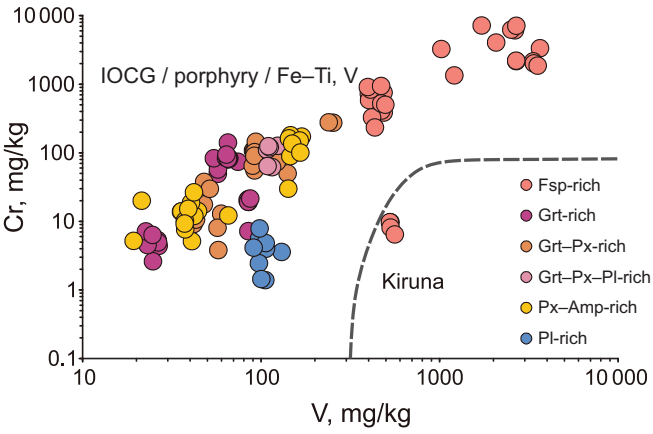

Fig. 11. V and Cr concentrations in Jõhvi magnetite, with fields for magnetite compositions of different genetic types after Knipping et al. (2015). Abbreviation: IOCG – iron oxide–copper–gold.

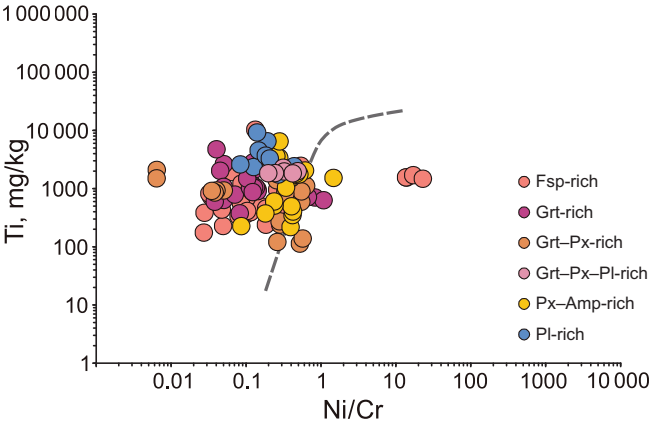

Fig. 12. Ti vs. Ni/Cr diagram of magnetite from the JMA (after Dare et al. 2014).

igneous field, but its Ti concentration (<2000 mg/kg) remains typical of hydrothermal magnetite. In contrast, igneous magnetite can reach Ti concentrations of up to ~100 000 mg/kg (Nadoll et al. 2015). Consistent with this, on a V vs. Cr plot, magnetite from the JMA plots away from the magmatic Kiruna-type field and instead aligns towards the IOCG and porphyry magnetite fields (Fig. 11; Knipping et al. 2015).

In contrast, the Ti vs. Ni/Cr plot of Dare et al. (2014) classifies most of the magnetite from the JMA as magmatic (Fig. 12). According to Dare et al. (2014), during the fractionation of intermediate to felsic magmas, Ni and Cr behave compatibly, yielding Ni/Cr ratios less than 1 in magnetite, whereas in hydrothermal systems, Ni is more soluble and decouples from Cr, resulting in Ni/Cr ratios greater than 1. By this criterion, the analysed magnetite would be considered magmatic. However, the use of the Ti vs. Ni/Cr diagram for magnetite provenance has been disputed (Pisiak et al. 2017; Frank et al. 2022). The apparent conflict between the classification by Dare et al. (2014) and the other lines of evidence presented above suggests that magnetite from the JMA underwent a multi-stage evolution.

5.4. Genetic interpretation of the JMA mineralisation

Bergslagen in central Sweden and possibly the Orijärvi district in southern Finland provide analogues for the geological setting of the JMA. These regions lie within the same crustal domain and contain similar volcanogenic–sedimentary and magmatic rock assemblages (Bogdanova et al. 2015; Nirgi and Soesoo 2021; Soesoo et al. 2021). A characteristic feature of the Bergslagen province is the close spatial association of Zn–Pb–Ag–(Cu–Au) sulphide deposits and magnetite-rich iron oxide deposits (Jansson and Allen 2013). The predominant deposits in Bergslagen are iron ores hosted in skarn and metacarbonate rocks, often rich in Mn, accompanied by various other ore types (Allen et al. 2003). These include BIFs, magnetite–calc-silicate skarns, manganiferous skarns, carbonate-hosted and apatite-bearing iron ores, stratiform Zn–Pb–Ag–(Cu–Au) sulphide bodies, and W-bearing skarns (Allen et al. 1996). Notably, individual deposits in Bergslagen can show features of multiple deposit types in different zones. Many iron oxide and base-metal skarns, especially those interlayered with volcanic strata, are interpreted as products of regional metamorphism affecting interbedded sedimentary, volcanic, and hydrothermally altered precursor rocks (Allen et al. 2003).

In this context, Soesoo et al. (2021) noted that JMA rocks preserve relics of banded iron formation, suggested by magnetite- and quartz-rich banding, and contain abundant aluminium-rich garnet. This supports a volcanogenic–sedimentary origin similar to that of an Algoma-type BIF. Our findings further support this interpretation, proposing that the iron mineralisation in the JMA was initially a volcanogenic hydrothermal BIF-type deposit and that the magnetite trace element signature was later modified by two major overprinting events: first, granulite-facies regional metamorphism, and second, metasomatic hydrothermal alteration associated with migmatisation, which caused partial melting and magnetite recrystallisation.

6. Conclusions

The trace element composition of magnetite in the Jõhvi magnetic anomaly (JMA) is strongly controlled by host-rock mineralogy. Principal component analysis identified distinct compositional populations characterised by systematic variations in Mn, V, Cr, Mo, Ti, and Ni.

Magnetite from Grt–Px-rich host rocks appears to be the least altered and therefore most likely to preserve the primary

geochemical signature of the original mineralisation. In contrast, magnetite hosted by Fsp-rich rocks records substantial modification associated with hydrothermal metasomatism and migmatisation.

Magnetite trace element discrimination methods did not yield a unique genetic classification for the JMA mineralisation. Depending on the discrimination scheme applied, magnetite compositions show affinities with porphyry, iron oxide–copper–gold (IOCG), hydrothermal banded iron formation (BIF), skarn, and other hydrothermal deposit types.

The Nadoll et al. (2014) discrimination scheme indicates that magnetite from the least altered Grt–Px-rich host rocks shows the closest affinity to hydrothermal BIF compositions. Together with geological, petrographic, and geochemical evidence, this supports an Algoma-type BIF origin for the JMA mineralisation that was subsequently modified by granulite-facies metamorphism and hydrothermal alteration associated with migmatisation.

The results demonstrate that magnetite trace element discrimination methods should be applied with caution in strongly overprinted systems. Metamorphic and hydrothermal processes can substantially modify primary trace element signatures, making robust genetic interpretations dependent on the integration of geochemical, petrographic, and geological evidence.

Data availability statement

Data not included in the paper or supplementary material will be made available upon request.

Acknowledgements

This research was funded by the Estonian Research Council's project TemTA-30 and supported by the Estonian Centre of Analytical Chemistry. The publication costs of this article were partially covered by the Estonian Academy of Sciences.

Supplementary online data

Supplementary online data to this article can be found at https://doi.org/10.3176/earth.2026.S09 and includes Table S1 detailing magnetite trace element concentrations.

References

Aitchison, J., Barceló-Vidal, C., Martín-Fernández, J. A. and Pawlowsky-Glahn, V. 2000. Logratio analysis and compositional distance. *Mathematical Geology*, **32**(3), 271–275. https://doi.org/10.1023/A:1007529726302

Allen, R. L., Lundstrom, I., Ripa, M. and Christofferson, H. 1996. Facies analysis of a 1.9 Ga, continental margin, back-arc, felsic caldera province with diverse Zn-Pb-Ag-(Cu-Au) sulfide and Fe oxide deposits, Bergslagen region, Sweden. *Economic Geology*, **91**(6), 979–1008. https://doi.org/10.2113/gsecongeo.91.6.979

Allen, R. L., Bull, S., Ripa, M. and Jonsson, R. 2003. *Regional Stratigraphy, Basin Evolution, and the Setting of Stratabound Zn–Pb–Cu–Ag–Au Deposits in Bergslagen, Sweden*. Final Report for SGU-FoU Project 03-1203/99. Geological Survey of Sweden and Boliden Mineral AB.

Beaudoin, G., Hébert, R., Wang, C. S. and Tang, J. 2005. Epithermal Au-Ag-Cu, porphyry Cu-(Au-Mo) and Cu-Au-Ag-Zn-Pb skarn deposits of the Gangdese Arc, Tibet. In *Mineral Deposit Research: Meeting the Global Challenge*. Springer, Berlin, Heidelberg, 1219–1222.

Bogdanova, S., Gorbatschev, R., Skridlaite, G., Soesoo, A., Taran, L. and Kurlovich, D. 2015. Trans-Baltic Palaeoproterozoic correlations towards the reconstruction of supercontinent Columbia/Nuna. *Precambrian Research*, **259**, 5–33. https://doi.org/10.1016/j.precamres.2014.11.023

Dare, S. A. S., Barnes, S.-J., Beaudoin, G., Méric, J., Boutroy, E. and Potvin-Doucet, C. 2014. Trace elements in magnetite as petrogenetic indicators. *Mineralium Deposita*, **49**(7), 785–796. https://doi.org/10.1007/s00126-014-0529-0

Dupuis, C. and Beaudoin, G. 2011. Discriminant diagrams for iron oxide trace element fingerprinting of mineral deposit types. *Mineralium Deposita*, **46**(4), 319–335. https://doi.org/10.1007/s00126-011-0334-y

Erisalu, E., Arvisto, E., Norman, A., Dantsenko, V., Koppelmaa, H., Niin, M. et al. 1969. *Отчёт по изучению кристаллического фундамента Йыхвиской магнитной аномалии и её окрестности (Report of the basement studies on Jõhvi magnetic anomaly and nearby)*. Geological Survey of Estonia, Kohtla-Järve, EGF 3032.

Frank, K. S., Spry, P. G., O'Brien, J. J., Koenig, A., Allen, R. L. and Jansson, N. 2022. Magnetite as a provenance and exploration tool for metamorphosed base-metal sulfide deposits in the Stollberg ore field, Bergslagen, Sweden. *Mineralogical Magazine*, **86**(3), 373–396. https://doi.org/10.1180/mgm.2022.39

Hagemann, S. G., Angerer, T., Duuring, P., Rosière, C. A., Figueiredo e Silva, R. C., Lobato, L. et al. 2016. BIF-hosted iron mineral system: a review. *Ore Geology Reviews*, **76**, 317–359. https://doi.org/10.1016/j.oregeorev.2015.11.004

Heinrich, C. A. 2007. Fluid-fluid interactions in magmatic-hydrothermal ore formation. *Reviews in Mineralogy and Geochemistry*, **65**(1), 363–387. https://doi.org/10.2138/rmg.2007.65.11

Jafari, A., Karimpour, M. H., Mazaheri, S. A., Malekzadeh Shafaroudi, A. and Ren, M. 2019. Geochemistry of metamorphic rocks and mineralization in the Golgohar iron ore deposit (No. 1), Sirjan, SE Iran: implications for paleotectonic setting and ore genesis. *Journal of Geochemical Exploration*, **205**, 106330. https://doi.org/10.1016/j.gexplo.2019.06.012

Jansson, N. F. and Allen, R. L. 2013. Timing and setting of skarn and iron oxide formation at the Smältarmossen calcic iron skarn deposit, Bergslagen, Sweden. *Mineralium Deposita*, **48**(3), 313–339. https://doi.org/10.1007/s00126-012-0432-5

Klein, C. 2005. Some Precambrian banded iron-formations (BIFs) from around the world: their age, geologic setting, mineralogy, metamorphism, geochemistry, and origin. *American Mineralogist*, **90**(10), 1473–1499. https://doi.org/10.2138/am.2005.1871

Knipping, J. L., Bilenker, L. D., Simon, A. C., Reich, M., Barra, F., Deditius, A. P. et al. 2015. Giant Kiruna-type deposits form by efficient flotation of magmatic magnetite suspensions. *Geology*, **43**(7), 591–594. https://doi.org/10.1130/G36650.1

Konhauser, K. O., Planavsky, N. J., Hardisty, D. S., Robbins, L. J., Warchola, T. J., Haugaard, R. et al. 2017. Iron formations: a global record of Neoarchaean to Palaeoproterozoic environmental history. *Earth-Science Reviews*, **172**, 140–177. https://doi.org/10.1016/j.earscirev.2017.06.012

Koppelmaa, H., Kivisilla, J., Klein, V. and All, T. 2002. *Geological Map of the Crystalline Basement of Estonia. Scale 1:400 000*. Geological Survey of Estonia, Tallinn.

Linari, A. A. 1940. *Aruanne sügavpuurimistest Jõhvi lähedal (Report on diamond drilling near Jõhvi). Tallinna Tehnikaülikooli toimetused*, **15**, 1–27.

Nadoll, P., Angerer, T., Mauk, J. L., French, D. and Walshe, J. 2014. The chemistry of hydrothermal magnetite: a review. *Ore Geology Reviews*, **61**, 1–32. https://doi.org/10.1016/j.oregeorev.2013.12.013

Nadoll, P., Mauk, J. L., Leveille, R. A. and Koenig, A. E. 2015. Geochemistry of magnetite from porphyry Cu and skarn deposits

in the southwestern United States. *Mineralium Deposita*, **50**(4), 493–515. https://doi.org/10.1007/s00126-014-0539-y

Nirgi, S. and Soesoo, A. 2021. Geology and geochemistry of a Paleoproterozoic iron mineralization in north-eastern Estonia. *Transactions of the Karelian Research Centre of the Russian Academy of Sciences*, **10**, 25–43. https://doi.org/10.17076/geo1492

Nirgi, S., Maala, L., Kaasik, T., Smyth, D. and Wrobel, F. 2022. *Assessment of the exploration potential of the Jõhvi magnetic anomaly, NE Estonia*. Report No 9552. Geological Survey of Estonia, Tallinn.

Pisiak, L. K., Canil, D., Lacourse, T., Plouffe, A. and Ferbey, T. 2017. Magnetite as an indicator mineral in the exploration of porphyry deposits: a case study in till near the Mount Polley Cu-Au deposit, British Columbia, Canada. *Economic Geology*, **112**(4), 919–940. https://doi.org/10.2113/econgeo.112.4.919

Plado, J., Kiik, K., Jokinen, J. and Soesoo, A. 2020. Magnetic anomaly of the Jõhvi iron ore, northeastern Estonia, controlled by subvertical remanent magnetization. *Estonian Journal of Earth Sciences*, **69**(4), 189–199. https://doi.org/10.3176/earth.2020.13

Puura, V. and Kuuspalu, T. 1966. *Eesti NSV metallogeeniline kaart mõõtkavas 1:500 000. Aruanne III. Maagi-ilmingud Jõhvi ja Uljaste ala kristalliinses vundamendis (Metallogenic map of the Estonian SSR at a scale of 1:500 000. Report III. Ore occurrences in the crystalline basement of the Jõhvi and Uljaste areas)*. Geoloogiafond, Tallinn.

Puura, V., Amantov, A., Tikhomirov, S. and Laitakari, I. 1996. Latest events affecting the Precambrian basement, Gulf of Finland and surrounding areas. *Geological Survey of Finland. Special Paper*, **21**, 115–125.

Skirrow, R. G. 2022. Iron oxide copper-gold (IOCG) deposits – a review (part 1): settings, mineralogy, ore geochemistry and classification. *Ore Geology Reviews*, **140**, 104569. https://doi.org/10.1016/j.oregeorev.2021.104569

Soesoo, A., Puura, V., Kirs, J., Petersell, V., Niin, M. and All, T. 2004. Outlines of the Precambrian basement of Estonia. *Proceedings of the Estonian Academy of Sciences. Geology*, **53**(3), 149–164. https://doi.org/10.3176/geol.2004.3.02

Soesoo, A., Nirgi, S. and Plado, J. 2020. The evolution of the Estonian Precambrian basement: geological, geophysical and geochronological constraints. *Transactions of the Karelian Research Centre of the Russian Academy of Sciences*, **2**, 18–33. https://doi.org/10.17076/geo1185

Soesoo, A., Nirgi, S., Urtson, K. and Voolma, M. 2021. Geochemistry, mineral chemistry and pressure–temperature conditions of the Jõhvi magnetite quartzites and magnetite-rich gneisses, NE Estonia. *Estonian Journal of Earth Sciences*, **70**(2), 71–93. https://doi.org/10.3176/earth.2021.05

Solano-Acosta, J. D., Soesoo, A. and Hints, R. 2023. New insights of the crustal structure across Estonia using satellite potential fields derived from WGM-2012 gravity data and EMAG2v3 magnetic data. *Tectonophysics*, **846**, 229656. https://doi.org/10.1016/j.tecto.2022.229656

Sundblad, K., Salin, E., Claesson, S., Gyllencreutz, R. and Billström, K. 2021. The Precambrian of Gotland, a key for understanding the Proterozoic evolution in southern Fennoscandia. *Precambrian Research*, **363**, 106321. https://doi.org/10.1016/j.precamres.2021.106321

Suuroja, K. 1969. *Jõhvi magnetiitse maagistumise iseloomust (On the nature of the Jõhvi magnetite mineralisation)*. BSc thesis. Tartu Ülikool, Tartu.

Tikhomirov, S. N. 1966. Геологическое строение докембрийского фундамента в пределах Ленинградской области и Прибалтики *(Geological structure of the Precambrian basement within the Leningrad Region and the Baltic area). VSEGEI, Leningrad.*

Vaganova, Z. and Kadõrova, M. 1948. *ENSV eelkambriumi kristalliinsed kivimid ja raudkvartsiidid Jõhvi linna süvapuuraukude materjalide alusel (Precambrian crystalline rocks and ferruginous quartzites of the Estonian SSR based on materials from deep boreholes in the town of Jõhvi)*. Geoloogiafond.

Vaher, R., Puura, V. and Erisalu, E. 1962. The tectonic pattern of Northeast Estonia. *ENSV TA Geoloogia Instituudi Uurimused*, **10**, 319–335.

Yıldırım, N., Dönmez, C., Kang, J., Lee, I., Pirajno, F., Yıldırım, E. et al. 2016. A magnetite-rich Cyprus-type VMS deposit in Ortaklar: a unique VMS style in the Tethyan metallogenic belt, Gaziantep, Turkey. *Ore Geology Reviews*, **79**, 425–442. https://doi.org/10.1016/j.oregeorev.2016.05.021

Magnetiidi jälgelemendid Jõhvi magnetiitgneissides: järeldused raua mineralisatsiooni tekkest ja hilisematest muutustest

Siim Nirgi, Alvar Ratt, Lennart Maala, Peeter Paaver, Alvar Soesoo ja Kalle Kirsimäe

Uurimistöö eesmärk oli selgitada Jõhvi magnetanomaaliat põhjustavate aluskorras levivate magnetiiti sisaldavate gneisside päritolu magnetiidis sisalduvate jälgelementide abil. Erinevates kivimtüüpides leiduvaid magnetiiditerasid analüüsiti petrograafiliselt ja nende keemiline koostis määrati LA-ICP-MS meetodiga. Jõhvi magnetiitide jälgelementide koostis viitab magnetiidi Algoma-tüüpi kihilise rauaformatsiooni (BIF) päritolule. Samas ei ole magnetiitide jälgelementide koostis erinevates kivimtüüpides ühtlane. Peakomponentide analüüs näitab, et jälgelemendid moodustavad kivimtüüpidega korreleeruvaid rühmi, mis viitab sellele, et magnetiidi jälgelementide muster ei kujunenud maagitekke käigus, vaid hilisemate moondeprotsesside mõjul ning sõltub magnetiidi ümbriskivimist. Granaat-pürokseengneissides leiduv magnetiit säilitab maagitekke primaarsed tunnused, samas kui päevakivirikastest kivimitest pärit magnetiit peegeldab tugevat sekundaarset metasomatismi ja migmatiseerumist. Jõhvi magnetiitgneisside kompleksis leviva magnetiidi muutlik jälgelementide koostis ja selle sõltuvus ümbriskivimist näitavad, et ainult magnetiidi geokeemia põhjal ei ole võimalik tugeva moonde läbinud kivimite algset maagitekke protsessi üheselt määrata.